CANDLE FLAMES IN NON-BUOYANT ATMOSPHERES

(Shortened Title: CANDLE FLAMES)

D. L. Dietrich* and H. D. Ross
NASA Lewis Research Center, Cleveland, Ohio

Y. Shu# and J. S. T'ien
Case Western Reserve University, Cleveland, Ohio

Currently with Diesel Cummings, Columbus, Indiana.

* Please address all correspondence to:

Daniel L. Dietrich
Mail Stop 110-3
NASA Lewis Research Center
21000 Brookpark Road
Cleveland, Ohio 44135
Phone: (216) 433-8759
FAX: (216) 433-3793
e-mail: daniel.dietrich@lerc.nasa.gov

ABSTRACT

This paper addresses the behavior of a candle flame in a long-duration, quiescent microgravity environment both on the space Shuttle and the Mir Orbiting Station (OS). On the Shuttle, the flames became dim blue after an initial transient where there was significant yellow (presumably soot) in the flame. The flame lifetimes were typically less than 60 seconds. The safety-mandated candlebox that contained the candle flame inhibited oxygen transport to the flame and thus limited the flame lifetime. The flames on the Mir OS were similar, except that the yellow luminosity persisted longer into the flame lifetime because of a higher initial oxygen concentration. The Mir flames burned for as long as 45 minutes. The difference in the flame lifetime between the Shuttle and Mir flames was primarily the re-designed candlebox that did not inhibit oxygen transport to the flame. In both environments, the flame intensity and the height-to-width ratio gradually decreased as the ambient oxygen content in the sealed chamber slowly decreased. Both sets of experiments showed spontaneous, axisymmetric flame oscillations just prior to extinction.

The paper also presents a numerical model of candle flame. The model is detailed in the gas-phase, but uses a simplified liquid/wick phase. The model predicts a steady flame with a shape and size quantitatively similar to the Shuttle and Mir flames. The model also predicts pre-extinction flame oscillations if the decrease in ambient oxygen is small enough.

INTRODUCTION

The behavior of a candle flame is the most common public inquiry about combustion in the absence of gravity. This is primarily because the candle flame is so familiar to everyone. From a fundamental perspective the candle flame is a complex combustion system. The fuel is a mixture of long chain- hydrocarbon molecules with complicated oxidation chemistry. The flame interacts with a porous wick, with intricate heat and mass transfer. Despite these complexities, candles offer such simplicity in experimental setup that they are used often to study a wide range of combustion phenomena such as flame flicker

(Buckmaster and Peters, 1986), spontaneous, near-extinction flame oscillations (Chan and T'ien, 1978), low-gravity smoke production (Urban et al., 1996), effects of electric fields (Carleton and Weinberg, 1989), elevated gravity (Villermaux and Durox, 1992), and magnetic fields (Lawton and Weinberg, 1969).

The candle flame in microgravity is uniquely stationary where, excepting Stefan flow, diffusion is the only trasport mechanism for fuel and oxygen to the flame and combustion products away from the flame. Both Carleton and Weinberg (1989) and Ross and co-workers (Ross et al., 1991a,b; Dietrich et al., 1994) studied the effects of reduced gravity on candle flames in both aircraft and drop tower facilities. The reduced gravity airplane tests typically produce fluctuating flames due to g-jitter, but on occasion show, consistent with drop tower studies, a nearly hemi-spherical flame. These tests, however, could not study the characteristics of the candle flame in a long-duration microgravity environment. We were interested in how long the candle flame could exist in the absence of gravity. We were also interested in the extinction behavior of the candle flame burning in a large sealed chamber in microgravity. We used the candle flame as the model diffusion flame and present the results of two sets of long-duration, quiescent, microgravity experiments. The first experiment flew aboard the Shuttle on the STS-50 (USML-1) mission in 1992. The second flight was on the Mir Orbiting Station (Mir OS) in 1995. This paper presents the results of the experiments and compares the results of the experiments to the predictions of a numerical model of the candle flame.

EXPERIMENTAL HARDWARE

Figures 1 and 2 show the hardware for the Shuttle and Mir experiments, respectively. The Shuttle hardware consisted of a perforated candlebox (11.5 cm on a side) made of a 0.95 cm thick polycarbonate, and a separate, manually operated igniter. The box, required by safety engineers, permitted fresh oxidizer to reach the candle but preempted the possibility of a crew-worn glove or other surrounding material from accidentally igniting. The ignition system was a loop of 250 μm aluminum alloy wire heated with a current of approximately 3

amperes. The crew manually ignited the candle and removed the hot-wire after ignition. The Shuttle's pressure and oxygen mole fraction were 1 atm and 0.217 at the time of each experiment.

The hardware was different for the second set of experiments on the Mir OS. The container was a 20 cm cube-shaped wire mesh screen as opposed to the perforated polycarbonate. The screen provided more than 50% free area (as opposed to less than 15% on the Shuttle experiment) yielding significantly less resistance for oxygen to diffuse to the flame and combustion products to diffuse away from the flame[1]. The ignition system was the same for the Mir experiments except that the igniter was automatically retracted after a preset ignition time (4-5 seconds for almost all tests), rendering the ignition a more repeatable process. The Mir operated at atmospheric pressure with an ambient oxygen mole fraction between 0.22 and 0.25.

The crew operated the experiments inside a glovebox facility. This facility provided a working volume (25 l on the Shuttle and 44 l on the Mir OS), video cameras and recording capabilities. The data from the Shuttle experiments were primarily video recordings from orthogonally located black and white video cameras and a few still color photographs. The primary data in the Mir experiments were audio recordings of crew observations and color photographs of the flame from a 35 mm SLR camera. The color video cameras in the Mir glovebox facility lacked the low-light sensitivity necessary to image the flames. In some of the Mir tests, the crew turned on the lights in the glovebox at various times to allow video observation of the liquefied wax.

The composition of the candle for both experiments was 80 percent (by weight) of an n-parrafin wax (typically C_{19}-C_{35} hydrocarbon) with 20 percent stearic acid ($C_{18}H_{36}O_2$) to impart toughness. The Shuttle experiments used 7 identical candles (approximately 2 mm wick diameter, 5 mm candle diameter, 12 mm candle length, and 3

---

1 The changes in the design were possible because the safety of the experiment was demonstrated on the Shuttle experiment.

mm initial exposed wick length). There were 79 total candles supplied with the hardware in the Mir experiments with three different wick diameters (approximately 1, 2 and 3 mm), two different candle diameters (5 and 10 mm) and two different lengths of initially exposed wick (3 and 6 mm) in the Mir experiments. All candles in the Mir tests were 2 cm in length (from the base of the solid wax to the tip of the wick).

A 3-axis accelerometer sampling at 125 Hz for the Shuttle experiments and 25 Hz for the Mir experiments was mounted underneath the floor of the glovebox working volume. Measured accelerations in both spacecraft were below 10^{-5} g_o (g_o being the accleration due to gravity at sea level) at frequencies below a few Hz, rendering effects of residual gravity and g-jitter unimportant in these tests.

EXPERIMENTAL OBSERVATIONS

Immediately after ignition, the candle flame in the Shuttle tests was spherical and bright yellow. After 8-10 seconds, the yellow, presumably from soot, disappeared, and the flame became blue and hemispherical with a diameter of approximately 1.5 cm (Figure 3(a)). These behaviors are consistent with the earlier, short-duration microgravity studies in aircraft (Carleton and Weinberg, 1989) and the NASA Lewis Research Center 5.2 second drop tower experiments (Ross et al., 1991a). After the ignition transient, the flame luminosity decreased continuously until extinction.

For the Mir experiments the flames were luminous and spherical immediately after ignition, resembling the Shuttle flames. Unlike on the Shuttle, however, the yellow luminosity often lasted for minutes into the flame lifetime. This was due to the increased oxygen concentration in the Mir OS. The entire mass of wax melted (but did not drip) within two minutes of ignition for the 5 mm diameter candles and within five minutes of ignition for the 10 mm diameter candles. The candle flame then looked as in Figure 3(b). Small bubbles, presumably from air that had been trapped inside the wick, circulated inside the liquid wax. This motion was the result of surface tension gradients (temperature gradients) along the surface of the liquid. At some point, this molten ball of wax suddenly

became unstable, collapsed and moved back along the candle holder as in Figure 3(c). The flame changed only slowly then until extinction.

For the Shuttle tests, extinction typically occurred between 40 and 60 seconds, except one flame that had a lifetime of 105 seconds. All of the candles in the Mir tests burned longer than the Shuttle candles. The flame lifetimes varied from over 100 seconds to over 45 minutes. For the Mir tests, the candles with the largest wick diameters typically had the shortest flame lifetimes and the candles with the smallest wick diameters typically had the largest.

In the Mir experiments, the crew switched the lights in the glovebox on after flame extinction, and a white, spherical cloud with a diameter 2-3 times that of the candle flame was present (Figure 3(d)). This cloud is probably a mist of condensed wax droplets (and possibly water droplets) that formed while wax continued to vaporize after the flame extinguished.

Each candle flame on the Shuttle oscillated spontaneously in the final 5 seconds. The flame traced symmetrically back and forth along the candle axis in each cycle (Figure 4). The top of the flame did not move during the oscillation. The base of the flame retreated and flashed back with a frequency of about 1 Hz with an amplitude that started small and grew until extinction. No oscillations occurred in any Mir tests with the smallest wick diameter, which was smaller than the wicks used in the Shuttle experiments. The flames in the Mir tests with the two larger wick diameters, however, did oscillate before extinction. The oscillation frequency was similar to that in the Shuttle experiments, only for a much longer period of time, up to 90 seconds.

Analysis of the video recordings for the Shuttle experiments and the 35 mm photographs for the Mir experiments yielded both the flame diameter, D (maximum visible flame dimension perpendicular to the candle axis), and height, H (maximum visible flame dimension parallel to the wick), as functions of time (see definition of H and D in Fig. 7). For the Shuttle experiments, there was no consistent behavior of the flames with respect to

H and D. The flame diameter and height sometimes increased with time and sometimes decreased with time. This was due to variations in the ignition procedure and in the initial ambient environment in the candlebox. Figure 5 shows D and H as a function of time for the three different wick sizes in the Mir experiments. The flame diameter and height in the Mir experiments always started small and increased with time. This consistency was the result of a more repeatable ignition method. The flame growth for the first 50-75 seconds for all of the candles in Figure 5 corresponds to the time for the solid wax to melt. Around this time, the liquid wax collapsed (Figures 3c and 3d), and afterward the flame size changed only slowly, if at all, with time. Additionally, Figure 5 shows that the larger the wick size, the larger the quasi-steady flame size, as expected.

For both the Shuttle and Mir experiments, the ratio H/D always decreased slightly with time (over the flame lifetime) and was quite repeatable from test to test. Figure 6 shows H/D as a function of time for a Shuttle test and two Mir tests. The candle diameter for each test in Figure 6 was 5 mm. One of the Mir tests in Figure 6 had the same wick (approximately 2 mm diameter) as the Shuttle test, and the other had the smaller wick size (approximately 1 mm diameter). While the values of the flame size of the Mir experiments were consistent with the Shuttle, the value of H/D is somewhat higher for the Mir tests. This latter observation is probably be due to the increased ambient oxygen concentration in the Mir tests. For the Mir experiment with the larger wick diameter in Figure 6, H/D increased slightly for the first 75 seconds, then decreased until extinction. The change in behavior at 75 seconds corresponds to the collapse of the liquid wax.

NUMERICAL MODEL

The numerical model of the candle flame is two-dimensional and axisymmetric in the gas-phase. While the model is relatively detailed in the gas-phase by considering finite-rate chemistry and radiative loss, the detailed heat and mass transfer processes occuring in the porous wick and solid wax are neglected. Specifically, we assume that the fuel

evaporates from a small porous sphere with constant radius, R, that is coated with a pure liquid fuel at its boiling temperature. This sphere is connected to an inert cone with a prescribed temperature distribution. The cone, which has a half angle of 23°, acts as a heat sink to simulate the flame quenching aspect of the candle wick and wax[2]. Figure 7 shows a schematic of the problem.

The mathematical formulation utilizes a two-dimensional spherical coordinate system. The gas-phase model assumes: one-step, second-order overall Arrhenius reaction, constant specific heats and thermal conductivity, constant Lewis number for each species (although different species can have different, constant Lewis numbers), ideal gas behavior and no buoyant force. The last assumption allows a simplified treatment of the momentum equation (Baum, 1994). This includes the assumption of potential flow and the product $(\bar{\rho}\,\bar{T})$ to be constant. Flame radiative losses from CO_2 and H_2O are accounted for by a gray gas treatment. The following non-dimensional variables are defined as (bars indicate dimensional quantities):

$$T=\frac{\bar{T}\bar{C}p}{\bar{q}},\quad r=\frac{\bar{r}}{\bar{R}},\quad \rho=\frac{\bar{\rho}}{\bar{\rho}_\infty},\quad t=\frac{\bar{t}\,\bar{\alpha}_\infty}{\bar{R}^2},\quad u_r=\frac{\bar{R}\,\bar{u}_r}{\bar{\alpha}_\infty},\quad u_\theta=\frac{\bar{R}\,\bar{u}_\theta}{\bar{\alpha}_\infty};$$

$$\phi=\frac{\bar{\phi}}{\bar{\alpha}_\infty},\quad \Phi=\frac{\bar{\Phi}}{\bar{\alpha}_\infty},\quad \omega_F=\frac{\bar{C}p\bar{R}^2}{\bar{\lambda}}\bar{\omega}_F,\quad L=\frac{\bar{L}}{\bar{q}},\quad E=\frac{\bar{E}\bar{C}p}{\bar{R}\bar{u}\bar{q}};$$

$$Da=\frac{\bar{\rho}_\infty^2\bar{C}p\bar{R}^2}{\bar{\lambda}}\bar{A};\quad q_r=\frac{\bar{R}^2\bar{C}p}{\bar{\lambda}\,\bar{q}}\bar{q}_r.,\quad \Phi=\phi-\frac{\bar{T}}{\bar{T}_\infty}.$$

The non-dimensional equations are:

$$\frac{1}{r^2}\frac{\partial}{\partial r}\left(r^2\frac{\partial\Phi}{\partial r}\right)+\frac{1}{r\sin\theta}\frac{\partial}{\partial\theta}\left(\frac{\sin\theta}{r}\left(\frac{\partial\Phi}{\partial\theta}\right)\right)=\frac{\omega_F-q_r}{T_\infty}$$

$$\rho\frac{\partial Y_i}{\partial t}+\rho\,u_r\frac{\partial Y_i}{\partial r}+\frac{\rho\,u_\theta}{r}\frac{\partial Y_i}{\partial\theta}-\frac{1}{Le_i r^2}\frac{\partial}{\partial r}\left(r^2\left(\frac{\partial Y_i}{\partial r}\right)\right)-\frac{1}{Le_i r\sin\theta}\frac{\partial}{\partial\theta}\left(\frac{\sin\theta}{r}\left(\frac{\partial Y_i}{\partial\theta}\right)\right)=\nu_i\omega_F$$

$$\rho\frac{\partial T}{\partial t}+\rho u_r\frac{\partial T}{\partial r}+\frac{\rho\,u_\theta}{r}\frac{\partial T}{\partial\theta}-\frac{1}{r^2}\frac{\partial}{\partial r}\left(r^2\frac{\partial T}{\partial r}\right)-\frac{1}{r\sin\theta}\frac{\partial}{\partial\theta}\left(\frac{\sin\theta}{r}\left(\frac{\partial T}{\partial\theta}\right)\right)=\omega_F-q_r$$

---

2 A cone rather than a rod is easier to prescribe in the spherical coordinate system used. Also, examination of the photos shows that the liquid ball of wax may more closely resemble a cone than a rod.

$$\bar{\omega}_F = Da\rho^2 Y_O Y_F \exp(-\frac{E}{T})$$

Φ is a coupling variable.

The gas-phase radiative loss term, q_r, is $q_r = \mathcal{A}\,\sigma\,(T^4 - T_\infty^4)$. The mean aborption coefficient, $\mathcal{A}$, is $\mathcal{A} = 0.4[P_{CO2}\,\mathcal{A}_p(CO2) + P_{H2O}\,\mathcal{A}_p(H2O)]$, where P_i is the partial pressure of species i and $\mathcal{A}_p(i)$ is the Planck-mean absorption coefficient of species i. The Planck-mean absorption coefficients are from Abu-Romia and Tien (1967). The multiplication factor of 0.4 reflects the non-optically thin nature of the flame and the possible overestimate of the Planck-mean absorption data (Liu, et al., 1981; Bedir, et al. 1997). The radiative loss from liquid surface is neglected.

The one-step reaction for the candle wax is $C_{25}H_{52} + 0.31\,C_{18}H_{36}O_2 + 46O_2$ ---> $30.58CO_2 + 31.58H_2O$. The physical properties of the candle wax are in the nomenclature. The activation energy, E, of the reaction is 30 kcal/mole. The pre-exponential factor, $\bar{A}$, is selected such that the limiting oxygen index for a candle with a 0.6 mm radius is 0.19 (mole fraction). The resulting value for $\bar{A}$ is 1.0 (10^{11}) $cm^3/(g\ s)$ which is quite reasonable.

The boundary conditions in non-dimensional form are:

at r = 1:

$T = T_b$

$-\partial Y_F/\partial r = \rho\, u_r (1 - Y_F)$

$\partial Y_i/\partial r = \rho\, u_r Y_i$ (i = O2, CO2, H2O)

$\partial\Phi/\partial r = (1/\rho L - 1/T_\infty)*\partial T/\partial r$

at $\theta = 157°$:

$T(r) = T_c + (r_c - r)/(r_c - 1)*(T_b - T_c)$ at $(1 < r < r_c)$

$T(r) = T_c$ at $(r_c < r < \infty)$

$\partial Y_i/\partial\theta = 0$ (i = F, O2, CO2, H2O)

$\partial\Phi/\partial\theta = -(1/T_\infty)*\partial T/\partial\theta$

at $r = \infty$:

$T = T_\infty$

$Y_{O2} = Y_{O2,\infty}$

$Y_i = 0$ (i = F, CO2, H2O)

$$\partial\Phi/\partial r = -(1/T_\infty)*\partial T/\partial r$$

at $\theta = 0$:

$$\partial T/\partial\theta = \partial\Phi/\partial\theta = \partial Y_i/\partial\theta = 0 \quad (i = F, O2, CO2, H2O)$$

The computations below are for a porous sphere radius, $\overline{R} = 0.6$ mm, $r_c = 3.2$ cm, and $\overline{T}_b = 620$ K. The temperature distribution boundary condition at $\theta = 157°$ and $r > 1$ simulates the temperature distribution of the wick and the molten wax.

Solution Procedure

The reduced momentum equation is solved using an efficient Poisson solver. The equations for temperature and species are solved numerically based on finite difference and time marching techniques. The explicit scheme is used for the unsteady terms, the central difference for the diffusion terms and the upwind difference for the convective terms. The computation typically starts with a 'hot' profile or a previously converged flame solution (not the same condition as the case to be computed) as the initial condition. A steady flame solution (or extinction) evolves from the time marching procedure.

The computation is carried out on a two-dimensional spherical non-uniform grid system. The number of grid points is 36 in the r-direction and 26 in the θ direction. The variable grid distribution satisfies different requirements. The highest concentration of grid points is placed near the spherical wick, the cone surface, and the reaction zone. Along the r-direction, the minimum cell size is 0.1 times the porous sphere radius close to the sphere surface and expands with increasing r. The far-field boundary conditions are sufficiently far from the flame at a non-dimensional radius, $r = 206$. A complete description of the model, boundary conditions and solution procedures is available in Shu (1998).

Numerical Results

The model predicts that the candle flame will reach a steady-state in an infinite ambient. The inner portion of the flame reaches steady-state within 10 seconds, but the outer portion takes tens of seconds to reach steady state (similar to King, 1996). The time

to reach steady state at an arbitrary radius, $\mathcal{L}$, roughly scales with the diffusion time estimates [$(\mathcal{L}^2/\bar{\alpha})$ or $(\mathcal{L}^2/\mathcal{D}_F$], where $\bar{\alpha}$ and $\mathcal{D}_F$ are the thermal diffusivity and fuel vapor diffusion coefficient, respectively. The model results indicate, in agreement with experimental observations, that it is possible to observe the approximate steady-state flame shape and dimension in short-duration drop towers for flames away from the extinction limit. It is, however, not possible to accurately determine the extinction limit in short microgravity tests because the flame is sensitive to the region outside the flame zone which takes much longer to develop.

Figure 8(a) shows the computed temperature profiles for a steady candle flame with $\bar{R}$=0.6 mm (corresponding to the small diameter wick in the experiment) and an ambient oxygen mass fraction, Y_{Oe} = 0.254 (typical of that in Mir at the time of the experiments). The maximum temperature is located on the symmetry axis ($\theta = 0°$), 5 mm from the center of the wick. The high temperature zone is quite large and diffuse, as is typical of flames in microgravity. The cold, inert cone creates a low temperature region close to the cone surface and has a large effect on the temperaure distribution. Figure 8(b) shows the contours of the fuel vapor reaction rate, $\bar{w}_F$, which is proportional to the rate of combustion heat release. Equation 5 shows that $\bar{w}_F$ is a function of the fuel and oxygen concentration as well as the temperature. The maximum $\bar{w}_F$ occurs at the side of the wick, instead of at the top where the temperature is a mazimum, because of the higher oxygen concentration at the side (Figure 8(c)).

Similar to Grayson et al. (1994), we can compare visible flame shapes using a reaction rate contour. Choosing $\bar{w}_F = 0.2\ (10^{-3})$ g/cm^{3}s, the contour resembles the visible candle flame in the experiment, although the model predicts a slight inward hook at the bottom not present in the experiment. The model predicts a steady D and H of 14.6 mm and 10.0 mm, respectively, in the constant oxygen ambient (as opposed to the slowly decreasing one in the experiment). This compares quite favorably with the experimental

values of 14.5 mm and 11.2 mm. The disagreement between the model and experiment is probably due to the spherical wick geometry in the model as opposed to the more cylindrical shape in the experiment.

Figure 9 shows the temperature , oxygen mass fraction, fuel mass fraction, and fuel vapor reaction rate as a function of radial distance from the center of the sphere at $\theta = 0°$. This figure clearly shows a single temperature peak, but two peaks in the reaction rate. The low peak is due to the quench zone at the base of the flame which enables oxygen to diffuse to the wick surface. This creates a pocket of low reactivity that peaks near the wick inside the main reaction zone(not above the threshhold for a visible flame though). Note that the location of the minimum oxygen concentration is not at the wick surface (as is the case with the spherically symmetric droplet in microgravity), but is located 3 mm away from the wick surface.

Figure 10 shows the reaction rate contours corresponding to three different ambient oxygen mass fractions. As the oxygen mass fraction decreases from 0.254 to 0.22, the contours at the centerline ($\theta = 0°$) move only slightly, but there is a substantial upward retreat of bottom portion of the flame. This is similar to the experiments, where as the ambient oxygen concentration slowly decreases, the flame height decreases (relative to the diameter). The other interesting feature of Figure 10 is that the flame size (D and H) decreases slightly with decreasing ambient oxygen mass fraction. This is in contrast with the experiments that show that the flame diameter remains relatively constant in the decreasing oxygen ambient of the glovebox. The reason for this disagreement is currently not known. The fact that the flame diameter decreases with decreasing ambient oxygen is in contrast with the spherically symmetric droplet theory where the flame size increases with decreasing ambient oxygen concentration. Numerical models of flame spread over a solid surface, however, show that flame size decreases with decreasing ambient oxygen concentration. It appears then that the candle flame shares some features of both systems.

The numerical model also predicts spontaneous flame oscillations near the extinction limit. The extinction condition is approached by imposing a step decrease of the ambient oxygen concentration on a previously steady flame. The step decrease in oxygen simulates the gradually decreasing oxygen concentration in the sealed glovebox in the experiment. If this step is too large (e.g. from $Y_{O\infty} = 0.22$ to 0.215) the flame extinguishes by a monotonic decrease of the flame temperature. If the step decrease is small (e.g. from $Y_{O\infty} = 0.22$ to 0.21875), however, the flame oscillates prior to extinction. The flame oscillation is not a steady-state phenomena, but occurs as the flame transitions from a stable, steady-state to a non-flammable state. In other words, the model does not predict a steady oscillation. The oscillation always leads to extinction. The amplitude of the oscillation increases with time until extinction occurs. The amplification rate of the oscillation is related to the step size of the ambient oxygen, with a smaller step resulting in a smaller amplification rate and more oscillations before extinction.

Figure 11 shows the temporal variation of temperature , oxygen mass fraction, fuel mass fraction, and fuel vapor reaction rate during the oscillation at one point in the flame. The frequency is approximately 0.7 Hz which is similar to the experimental results. This is also close to the estimated fuel vapor diffusion time given by $[(D/2)^2/\mathcal{D}_F]$ (Dietrich et al., 1994) where $\mathcal{D}_F$ is the fuel vapor diffusion coefficient and (D/2) is the flame radius. The model results (Shu, 1998) show that the frequency of the oscillation increases as the fuel Lewis number decreases ($\mathcal{D}_F$ increases), or the flame radius decreases (smaller porous sphere). This is consistent with the time scale estimate above.

Figure 12 shows the movement of the visible flame for 1.875 seconds during one half of an oscillation cycle that starts3.375 seconds before flame extinction. The oscillation affects the entire flame. There is a variation of the flame width and an up-and-down motion near the bottom portion of the flame. The latter is qualitatively consistent with the experiment, although the magnitude of the movement is much greater in the experiment. This is probably due to the difference in the wick geometry. Specifically, the cylindrical

wick in the experiment allows a more extended evaporating surface in the vertical direction as compared to the spherical wick in the model.

DISCUSSION

The results show that the candle flames in the Mir tests had much longer lifetimes than those on the Shuttle. The Shuttle candle flames extinguished because of a lack of oxygen in the vicinity of the flame. This was not due to oxygen depletion inside the sealed glovebox, but because of the restriction to oxygen transport from the ambient through the perforated polycarbonate box. The difference in the ambient oxygen mole fraction between the Shuttle tests (0.217) and the Mir tests (0.225 to 0.249) would not extend the lifetimes by a factor of 10 or more, as the experiments showed. Thus, the predominant reason for the observed increase in flame lifetime for the Mir tests was the diminished resistance to oxygen transport through the container. The Mir candle flames extinguished primarily because of a lack of fuel. When the wax 'collapsed' and moved back along the candle holder, it was not in close proximity to the wick. As a result, this fuel was unavailable for burning. For nearly all of the candles, there was a film of wax surrounding the candle holder after the flame extinguished.

Given a flame lifetime of up to 45 minutes, we believe that the gas-phase was quasi-steady, implying that the flame was steady over a time period much longer than any reasonable characteristic gas-phase transport time. The numerical model predicts that a steady-state candle flame will exist in air. The model results show that the time to reach quasi-steady behavior for the gas-phase region in the vicinity the flame is less than 10 seconds. Further outside the flame the time to steady-state may be on the order of 100 seconds, but the changes in the flame as gauged by the fuel vapor reaction rate contours are small during this time. This is in good agreement with previous drop tower and these space-based experiments . Visually, the candle flame reaches a quasi-steady size, shape and color within 10 seconds. The changes that occur during longer time-scales are not the

result of an inherent gas-phase unsteadiness in a pure diffusion flame, but are from unsteady behavior in the solid/liquid phase and/or as a result of the gradually decreasing oxygen concentration in the sealed-glovebox volume.

Spontaneous oscillations are inherent to the near-extinction burning of these flames. The apparent dependence of the existence of oscillations on wick diameter in the experiments, implying a dependence on flame size, suggests that flame radiative losses may contribute to the onset of oscillations. Cheatham and Matalon (1996, 1997) recently investigated the mechanism of near-limit flame oscillations in the spherical droplet . They determined a stability boundary with heat loss and Lewis number as coordinates. When the heat loss is zero (adiabatic case), the Lewis number must be much larger than unity to have an oscillation. With increasing heat loss, the critical Lewis number decreases and can be less than unity with a sufficiently large heat loss rate. While we have not tried to verify the entire stability boundary (this would be very expensive using the present numerical model), we have made some comparrisons.

The oxygen and fuel Lewis numbers in the present model are 1.11 and 2.5, respectively. With the Lewis numbers in the model equal to each other and the value used by Cheatham and Matalon, the existence of oscillations also depends on the magnitude of the heat loss. Specifically, for $\overline{R} = 0.6$ mm, the model predicts a non-oscillatory, monotonic temperature decrease leading to extinction in the absence of radiative loss ($q_r = 0$). This is regardless of the step decrease in ambient oxygen concentration (a step decrease as low as 0.025 was tested). With heat loss included, however, the flame oscillates before extinction (the case presented above). This result is consistent with the results of Cheatham and Matalon. A number of previous theories (e.g. Kirkby and Schmitz, 1966; Baliga and T'ien, 1974) point out the possibility of near-limit oscillations with heat loss. These theories did not investigate the effect of Lewis number, but they do represent different types of flames (one-dimensional planar flame in Kirkby and Schmitz, and one-dimensional, premixed, solid-propellant flame in Baliga and T'ien). All of these

results suggest that heat loss plays an essential role in the occurrence of near-limit flame oscillations.

ACKNOWLEDGMENTS

The authors would like to extend special thanks to mission specialists Carl Meade and Bonnie Dunbar for performing the space Shuttle experiments and to Shannon Lucid for performing the Mir experiments. We also thank David Frate for his assistance in the preparation of the hardware for the Mir experiments. Peter Struk is thanked for his help in the analysis of the Shuttle data.

REFERENCES

Abu-Romia, M.M. and Tien, C.L. (1967). Appropriate Mean Absorption Coefficient for Infared Radiation of Gases. *ASME Journal of Heat Transfer* **89C**, 321.

Baliga, B.R. and T'ien, J.S. (1975). Unsteady Effects on Low-Pressure Extinction Limit of Solid Propellants. *AIAA Journal*. **13**, 1653.

Baum, H.R. (1994). Modeling Low Reynolds Number Microgravity Combustion Problems. *Modeling in Combustion Science* , edited by Buckmaster, J. and Takeno, T., Springer, 118.

Bedir, H., T'ien, J.S. and Lee, H.S. (1997). Comparison of Different Radiation Treatments for One Dimensional Diffusion Flame. Fall Technical Meeting of the Eastern States Section of the Combustion Institute, Princeton, New Jersey.

Buckmaster, J. and Peters, N. (1986). The Infinite Candle and its Stability - A Paradigm for Flickering Diffusion Flames. *Twenty-First Symposium (International) on Combustion* / The Combustion Institute, Pittsburgh, Pennsylvania, 1829.

Carleton, F. and Weinberg, F. (1989). Electric Field-Induced Flame Convection in the Absence of Gravity. *Nature* **330**, 635.

Chan, W.Y. and T'ien, J.S. (1978). An Experiment on Spontaneous flame Oscillation Prior to Extinction. *Combust. Sci. Tech.* **18**, 139.

Cheatham, S. and Matalon, M. (1996). Near Limit Oscillations of Spherical Diffusion Flames. *AIAA Journal* **34**(7), 1403.

Cheatham, S. and Matalon, M. (1997). Heat Loss and Lewis Number Effects on the Onset of Oscillations. *Twenty-SixthSymposium (International) on Combustion* / The Combustion Institute, Pittsburgh, Pennsylvania, 1063.

Dietrich, D.L., Ross, H.D. and T'ien, J.S. (1994). Candle Flames in Weakly Buoyant and Non-Buoyant Atmospheres. AIAA-94-0429, 32nd Aerospace Sciences Meeting and Exhibit, Reno, Nevada.

Grayson, G.D., Sacksteder, K.R., Ferkul, P.V. and T'ien, J.S. (1994). Flame Spreading Over a Thin Solid in Low-Speed Concurrent Flow - Drop Tower Experimental Results and Comparison with Theory. Microgravity Sci. Tech. **VII/2**, 182

King, M. (1996). An Unsteady Analysis of Porous Sphere and Droplet Fuel Combustion Under Microgravity Conditions. *Twenty-Sixth Symposium (International) on Combustion* / The Combustion Institute, 1227.

Kirkby, L.L. and Schmitz, R.A. (1966). An Analytical Study of the Stability of a Laminar Diffusion Flame. *Combust. Flame* . **10**, 205.

Lawton, J., and Weinberg, F.J. (1969). *Electrical Aspects of Combustion* . Clarenton, Oxford, pp. 336-340.

Liu, K.V., Lloyd, J.R. and Yang, K.T. (1981) An Investigation of Laminar Diffusion Flame Adjacent to a Vertical Flat Plate Burner. *International Journal of Heat and Mass Transfer* **24**(12), 1959.

Ross, H.D., Dietrich, D.L. and T'ien, J.S. (1991b) Observations of Candle Flames in Low Pressure and Low Gravity. Fall Technical Meeting of the Eastern States Section of the Combustion Institute, Orlando, Florida.

Ross, H., Sotos, R. and T'ien, J.S. (1991a). Observations of Candle Flames Under Various Atmospheres in Microgravity. *Combust. Sci. Tech.* **75**, 155.

Shu (1998) Modelling of Candle Flame and Near-Limit Oscillation in Microgravity. MS Thesis, Case Western Reserve University.

Urban, D.L., Griffin, D.W. and Gard, M.Y. (1996). Comparative Soot Diagnostics: Preliminary Results. NASA CP 10194, Fourth International Microgravity Combustion Workshop, 205.

Villermaux, E. and Durox, D. (1992). On the Physics of Jet Diffusion Flames. *Combust. Sci. Tech.* **84**, 279.

LIST OF FIGURES

NOMENCLATURE

$\bar{\alpha}$	gas-phase thermal diffusivity.
$\mathcal{A}$	mean absorbtion coefficient.
$\bar{A}$	pre-exponential factor (1×10^{11} $cm^3/g\ s$).
$\mathcal{A}_{Pi}$	Planck mean absorbtion coefficient for species i.
$\bar{Cp}$	gas-phase specific heat (0.334 cal/g K).
D	Flame diameter.
$\mathcal{D}$	Gas phase diffusion coefficient.
Da	Damkohler number.
$\bar{E}$	activation energy (3×10^4 cal/mole).
H	Flame height.
ϕ	velocity potential.
$\mathcal{L}$	Arbitrary radius.
$\bar{\lambda}$	gas-phase thermal conductivity (1.87×10^{-4} cal/K s cm).
$\bar{L}$	latent heat of vaporization (296.12 cal/g).
P_i	partial pressure of species i.
θ	angular coordinate.
$\bar{q}$	heat release per unit mass of fuel (10170 cal/g).
$\bar{\rho}$	gas density.
$\bar{r}$	radial coordinate.
$\bar{R}$	radius of the porous sphere.
R°	universal gas constant.
$\bar{T}$	temperature.
$\bar{t}$	time.
$\bar{u}$	velocity.
$\bar{w}_F$	fuel vapor reaction rate per unit volume.
Y	mass fraction.

Subscripts

b	boiling point of the fuel.
c	cold point of the rod.
CO2	carbon dioxide.
F	fuel.
H2O	water vapor.
O	oxygen.
θ	θ direction.
r	radial direction.
∞, e	ambient.

C-92-813

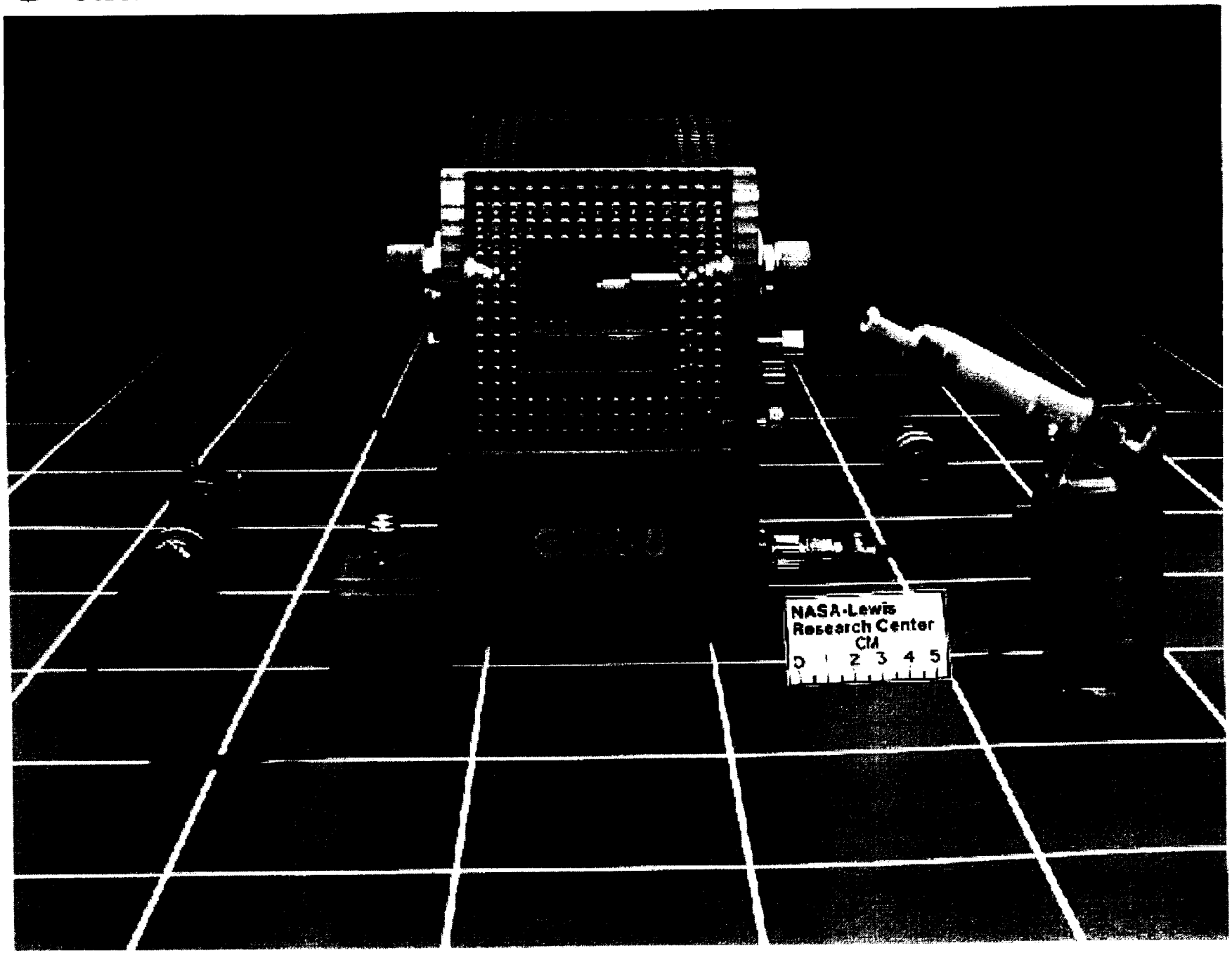

National Aeronautics and Space Administration
Lewis Research Center

C-95-1644

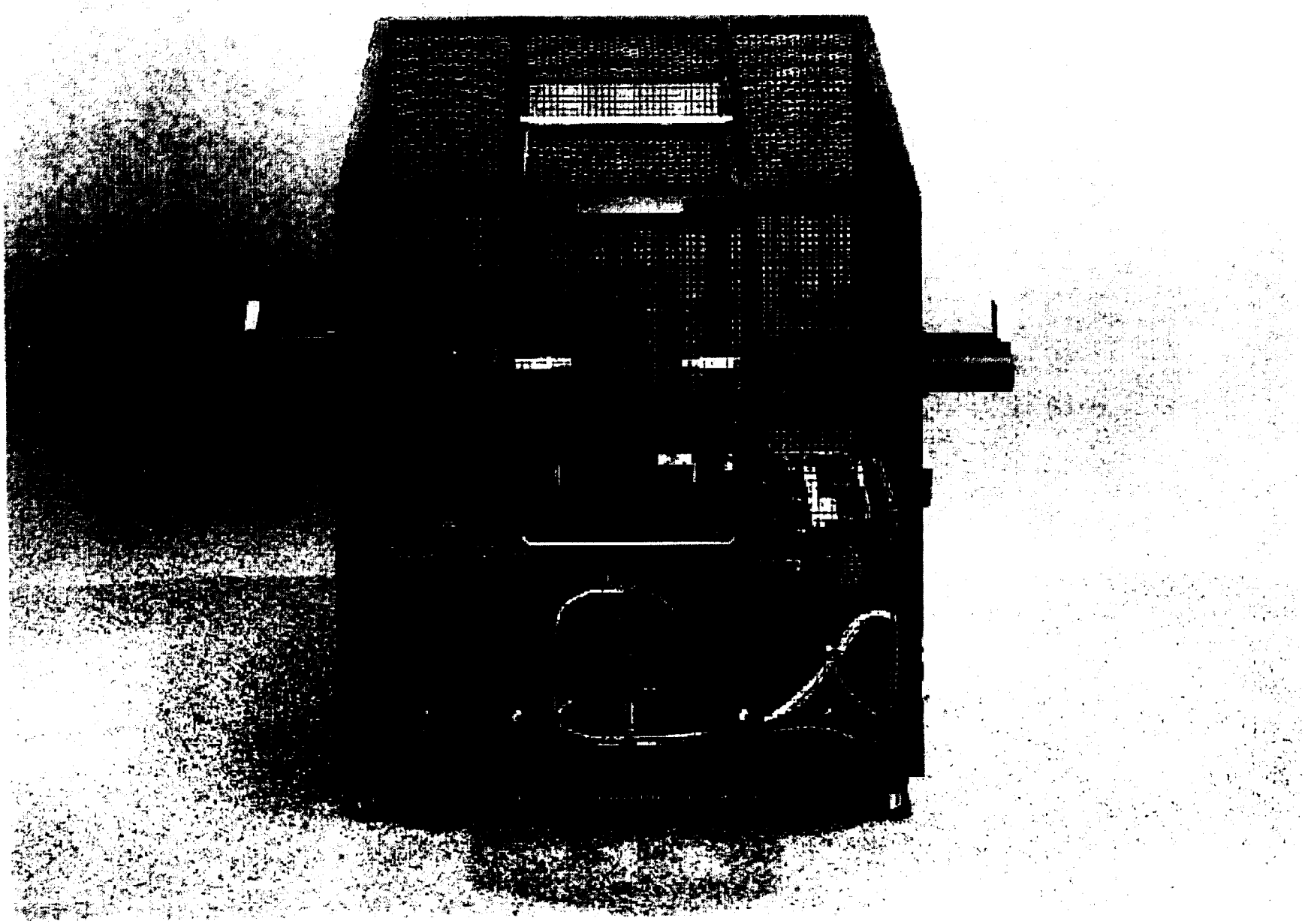

National Aeronautics and Space Administration
Lewis Research Center

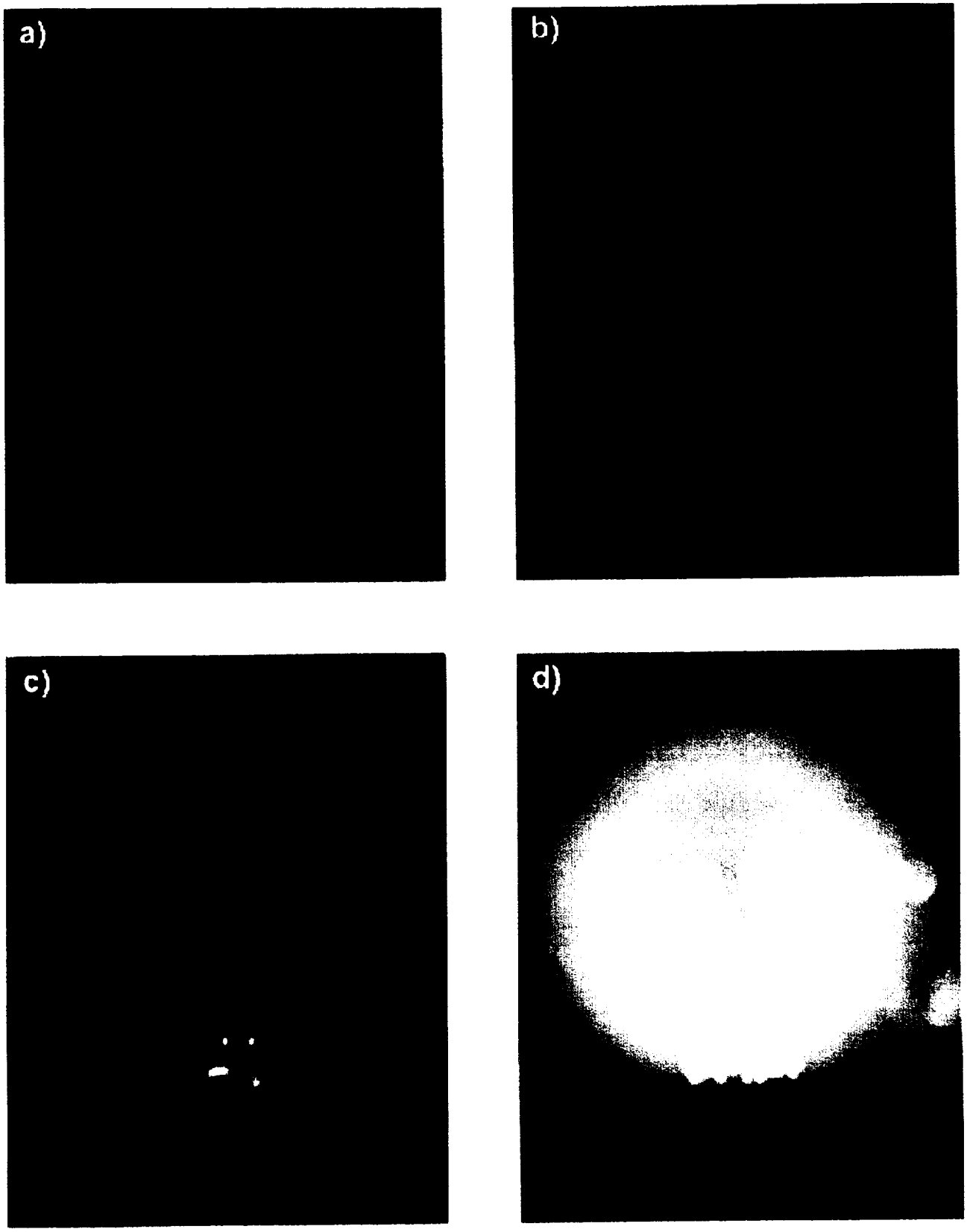

National Aeronautics and Space Administration
Lewis Research Center

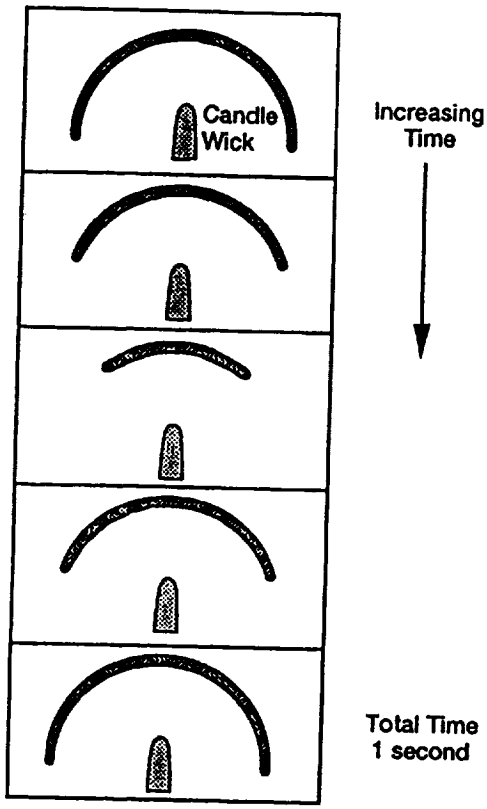

Figure 4. Schematic of pre-extinction flame oscillation.

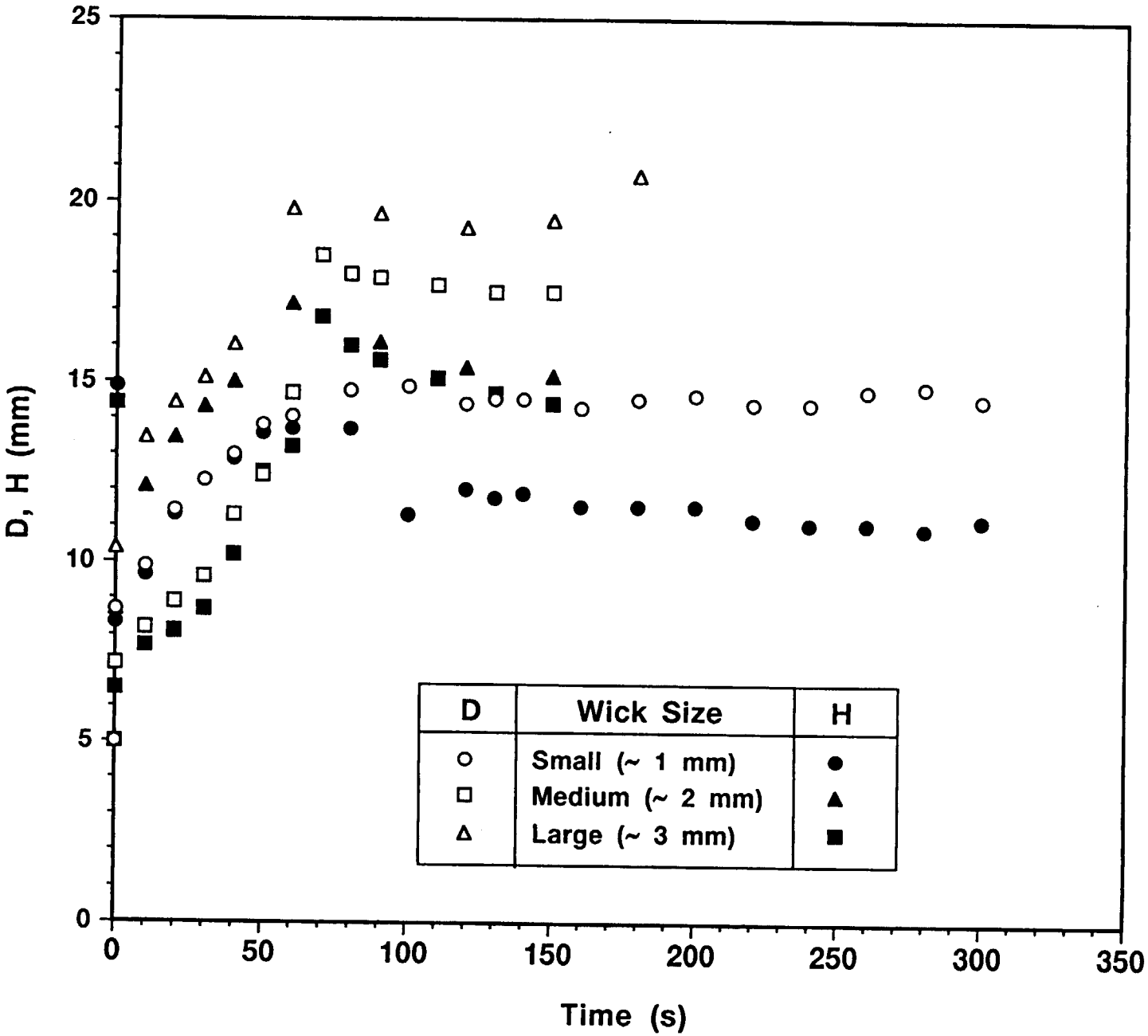

Figure 5. Flame diameter, D, and height, H, as a function of time for the 3 different wick sizes from the Mir experiments. The candle diameter was 5 mm in all three cases.

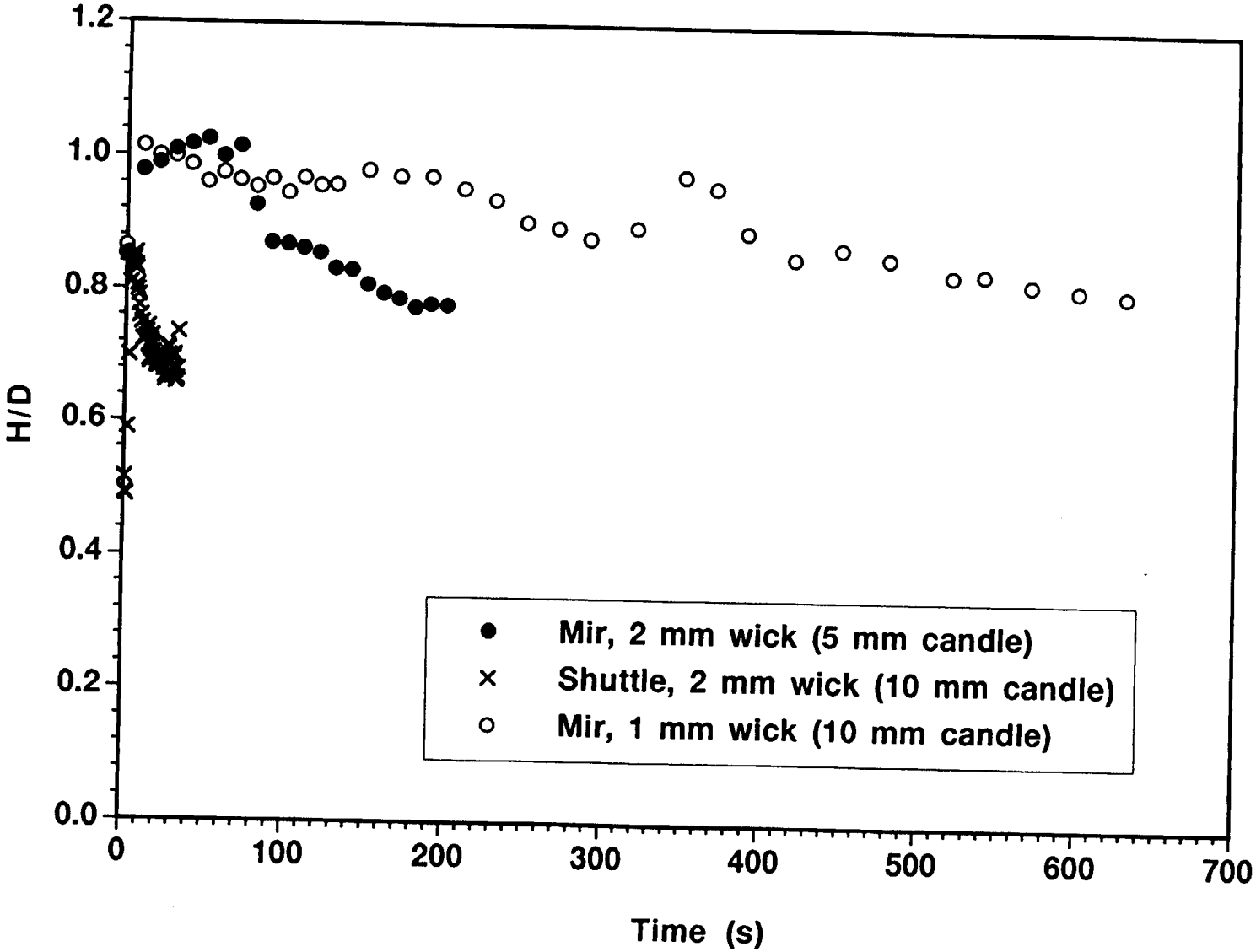

Figure 6. Flame shape, H/D, as a function of time for a typical Shuttle experiment and two Mir experiments (with different wick sizes).

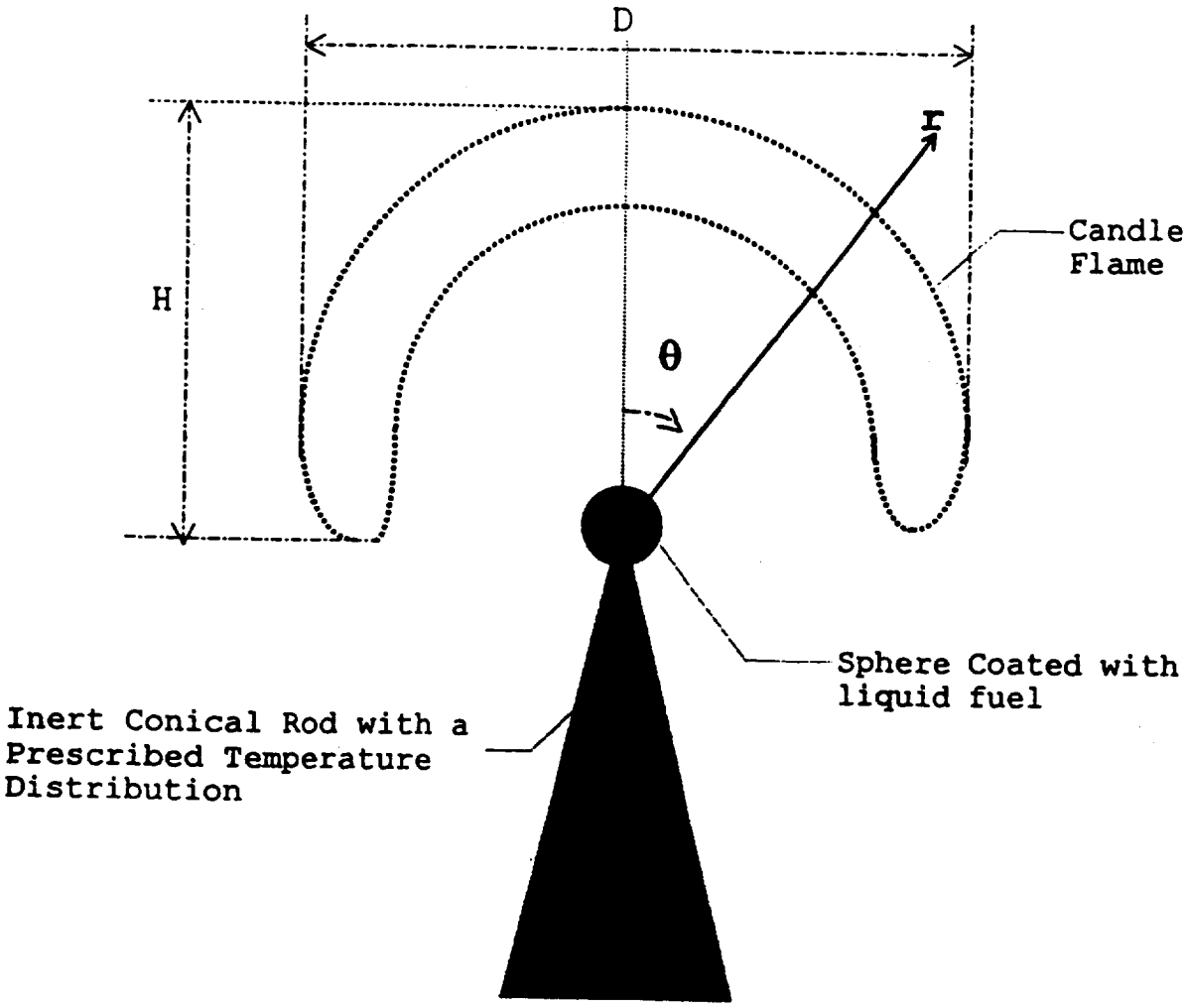

Figure 7. Schematic of the simplified candle in the numerical model.

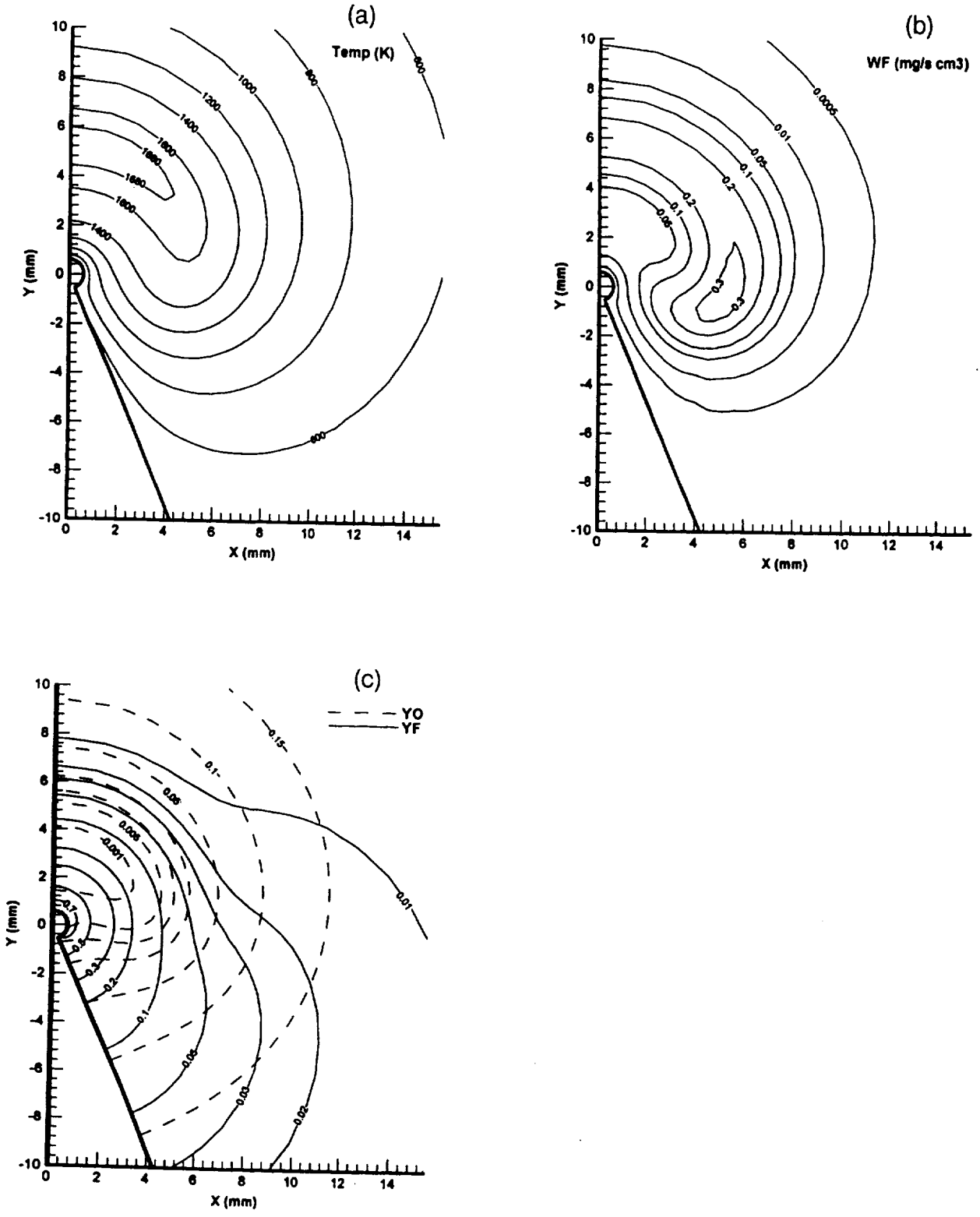

Figure 8. Numerical results for a candle flame in a YOe = 0.254 ambient, with $\overline{R}$ = 0.6 mm. 8a) Temperature ($\overline{T}$) contours; 8b) Fuel vapor reaction rate ($\overline{w}F$) contours; 8c) Oxygen (YO) and fuel (YF) mass fraction contours.

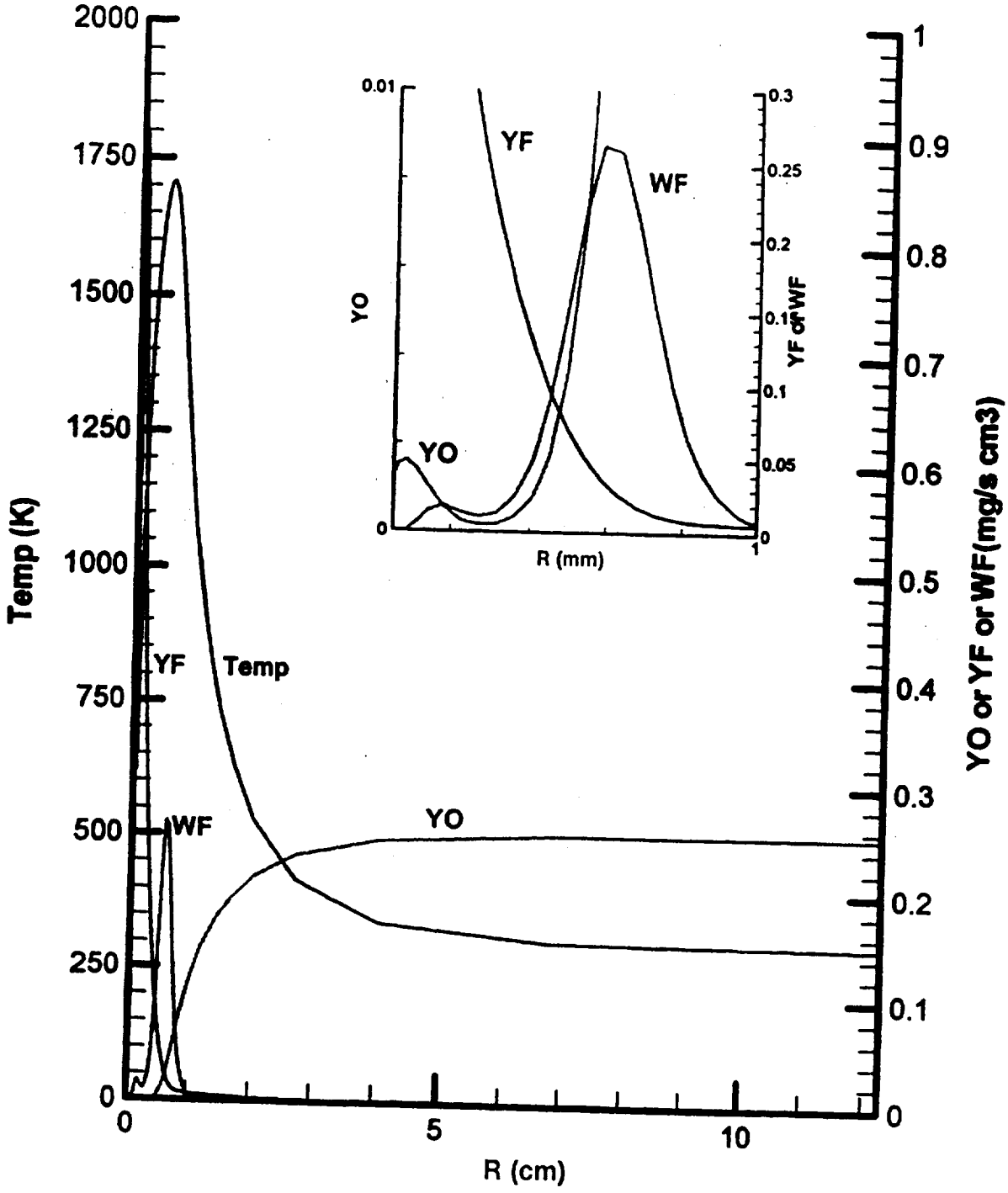

Figure 9. Radial contours of temperature ($\overline{T}$), oxygen mass fraction (YO), fuel vapor reaction rate ($\overline{wF}$), and fuel mass fraction (YF) at 0° for a candle in a YOe = 0.254 ambient, with $\overline{R}$ = 0.6 mm.

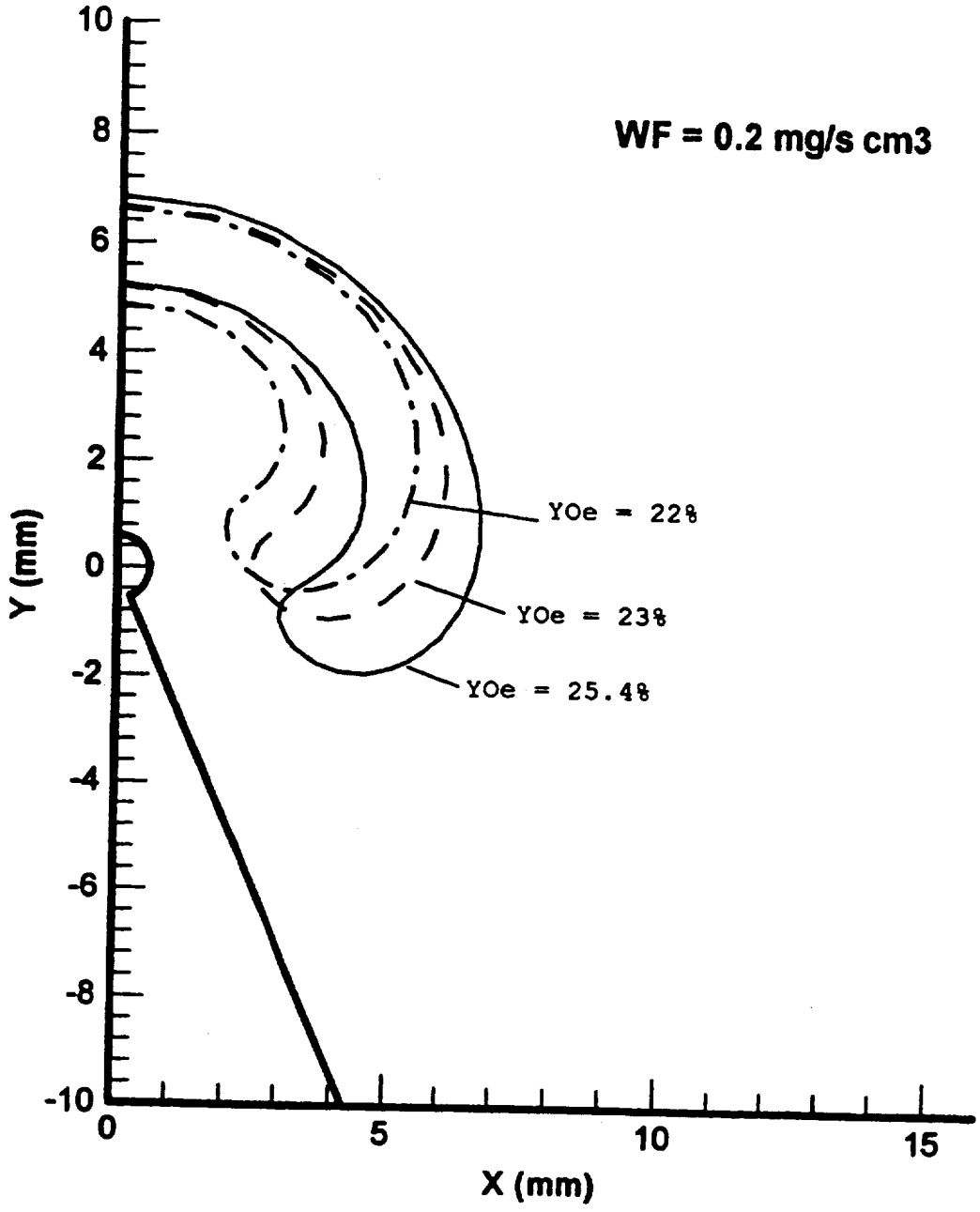

Figure 10. Fuel vapor reaction rate ($\bar{w}F$) contours for a candle with $\bar{R}$ = 0.6 mm in three different oxygen mass fraction ambients (YOe = 0.232, 0.254, 0.276).

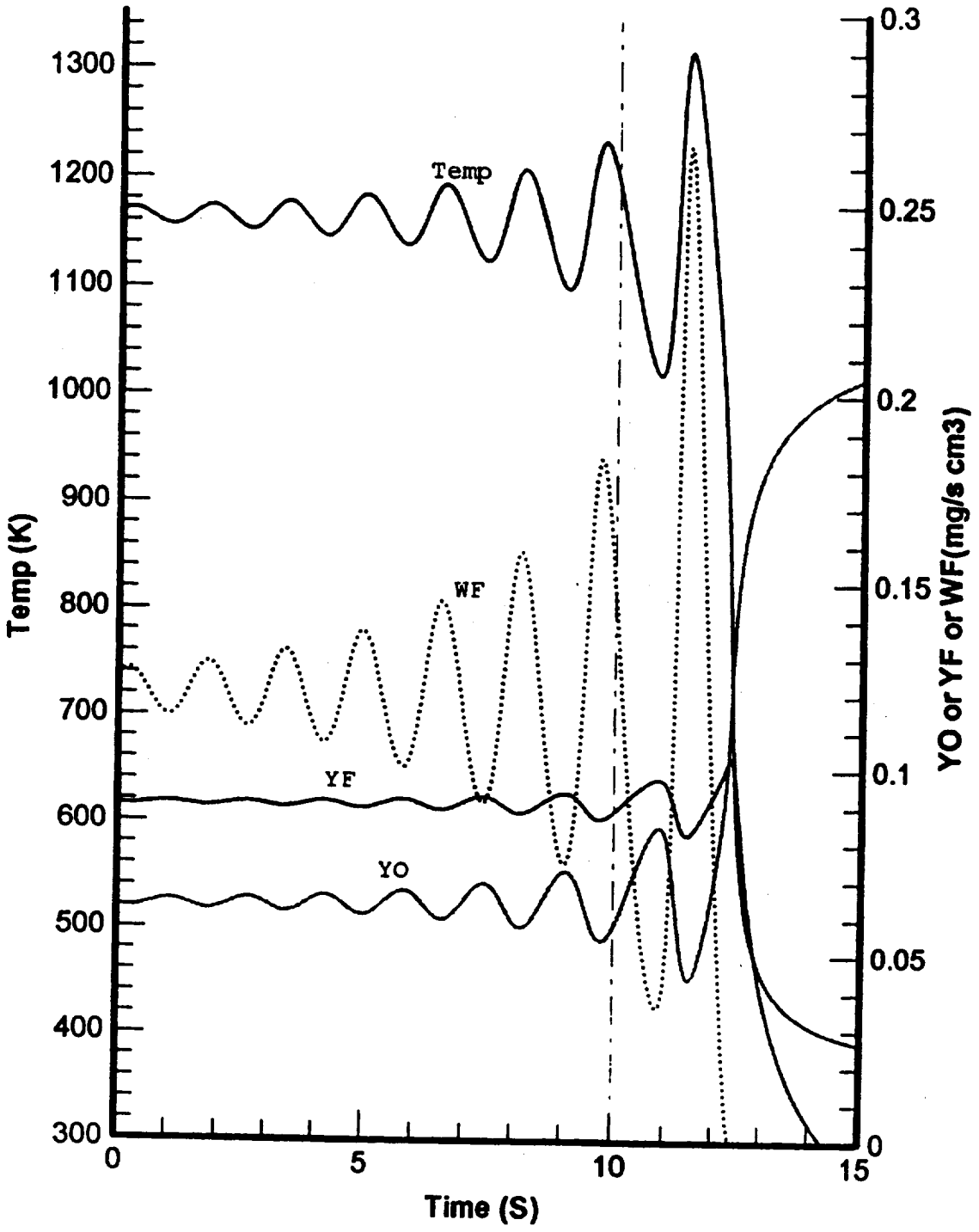

Figure 11. Temporal variation of temperature ($\overline{T}$), oxygen mass fraction ($\overline{YO}$), fuel vapor reaction rate (wF), and fuel mass fraction (YF) at a point in a candle flame (R = 0.6 mm) during a pre-extinction flame oscillation.

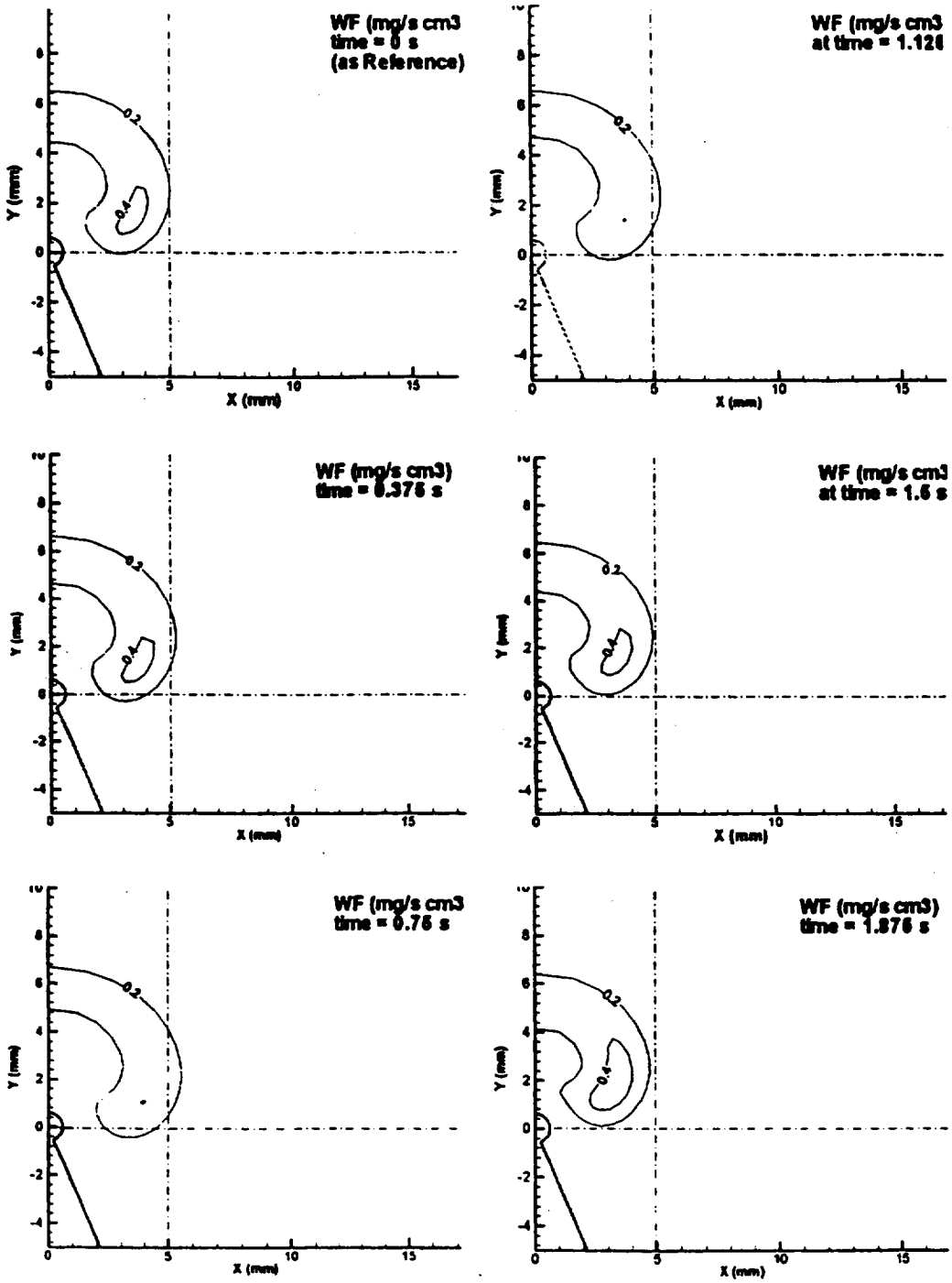

Figure 12. Fuel vapor reaction rate ($\overline{w}F$) contours for 1.875 seconds during one half of an oscillation cycle 3.375 seconds before extinction.